Mathematical Modeling of the Partial Hydrogenation of Vegetable Oil in a Monolithic Stirrer Reactor

Diego E. Boldrini, Daniel E. Damiani, and Gabriela M. Tonetto
PLAPIQUI (UNS-CONICET), Camino "La Carrindanga" Km 7, CC 717, CP 8000, Bahía Blanca, Argentina

DOI 10.1002/aic.14539
Published online July 2, 2014 in Wiley Online Library (wileyonlinelibrary.com)

Experimental and theoretical studies on the partial hydrogenation of vegetable oil in a monolithic stirrer reactor are reported. A complete mathematical model of the reactor was developed, including hydrogenation and isomerization kinetics, catalyst deactivation, external gas–liquid and liquid–solid as well as internal mass transfer. The experimental studies were carried out in a $Pd/Al_2O_3/Al$ monolithic stirrer reactor, at a wide range of temperatures (353–373 K), pressures (414–552 kPa), and catalyst loadings (0.00084–0.00527 $kg_{Pd,exp}$ m^{-3}). Based on this model, simulated data can be used to evaluate the catalyst ($Pd/Al_2O_3/Al$) and the hydrogenation process in consecutive catalytic tests under different operating conditions. © 2014 American Institute of Chemical Engineers *AIChE J*, 60: 3524–3533, 2014
Keywords: monolithic stirrer reactor, mathematical modeling, kinetics, mass transfer, hydrogenation, catalyst deactivation, palladium

Introduction

Monolithic catalysts have been studied for multiphase catalytic applications,[1,2] including hydrogenation reactions.[3–9] Considering that many of these reactions are limited by mass-transfer resistance phenomena, the excellent characteristics of monoliths associated with mass transport are of great relevance.

The hydrogenation of vegetable oils is the most commonly used method in the food industry to increase the melting point and oxidative stability of the end product. However, the use of vegetable oils for nonfood applications such as lubricants, paints, and plastics, which have traditionally been derived from crude oil, is gaining importance.[10–12] Even though biolubricants are more expensive than mineral-based lubricants, they are biodegradable and have low-toxicity. Nevertheless, partial hydrogenation of the vegetable oil is essential because of the requirement of higher viscosity and stability for oxidative rancidity and hydrolysis.

The industrial hydrogenation of vegetable oils is carried out in conventional slurry reactors operating in batch or semibatch mode.[13] Usually, the catalyst is nickel and the reaction is limited by gas mass transfer. In this process, most of the global resource consumption of the plant is used to remove the catalyst particles during the filtration process, and the remaining traces of the metal leached from the catalyst, by a series of consecutive bleaching stages. The final stage consists in the removal of the residual filter cake that remains after the previous steps. The contribution of these stages to the global costs of the process is usually significant, representing about 20% of the global operational expenses, but they can reach up to 50% of total costs if the hydrogen and catalyst consumption is excluded.[6]

Various alternative designs based on monolithic catalysts have been recently proposed as a potential solution to these problems,[14–17] simplifying the process and significantly reducing the operational costs.

In a previous work, palladium structured catalysts of anodized aluminum ($Pd/Al_2O_3/Al$) were evaluated as monolithic stirrers in the partial hydrogenation of sunflower oil.[8] The monolithic catalysts showed high activity, which decreased after consecutive uses. The excellent catalytic activity and mechanical stability of this structured catalyst promoted a deeper study of the reaction system.

A complete mathematical model of the reactor was developed, including hydrogenation and isomerization kinetics, catalyst deactivation, external gas–liquid and liquid–solid as well as internal mass transfer. The experimental studies were carried out in a $Pd/Al_2O_3/Al$ monolithic stirrer reactor, at a wide range of temperatures (353–373 K), pressures (414–552 kPa), and catalyst loadings (0.00084–0.00527 $kg_{Pd,exp}$ m^{-3}). The mathematical model could be used to evaluate the novel catalyst and the hydrogenation process in consecutive catalytic tests under different operating conditions.

Experimental

Catalyst preparation

Anodized aluminum monolithic catalysts were prepared using a commercial laminated pure aluminum as metallic substrate. The composition of the aluminum sheets was: 99.05 % wt Al, 0.4 % wt Fe, 0.25 % wt Si, 0.3 % wt others.

Anodizing technology was used to generate an alumina layer on the Al surface that would serve as support for the palladium catalyst. The anodization process was carried out with oxalic acid (1.6 M) as electrolyte at 313 K for 40 min

Additional Supporting Information may be found in the online version of this article.

Correspondence concerning this article should be addressed to G. M. Tonetto at gtonetto@plapiqui.edu.ar.

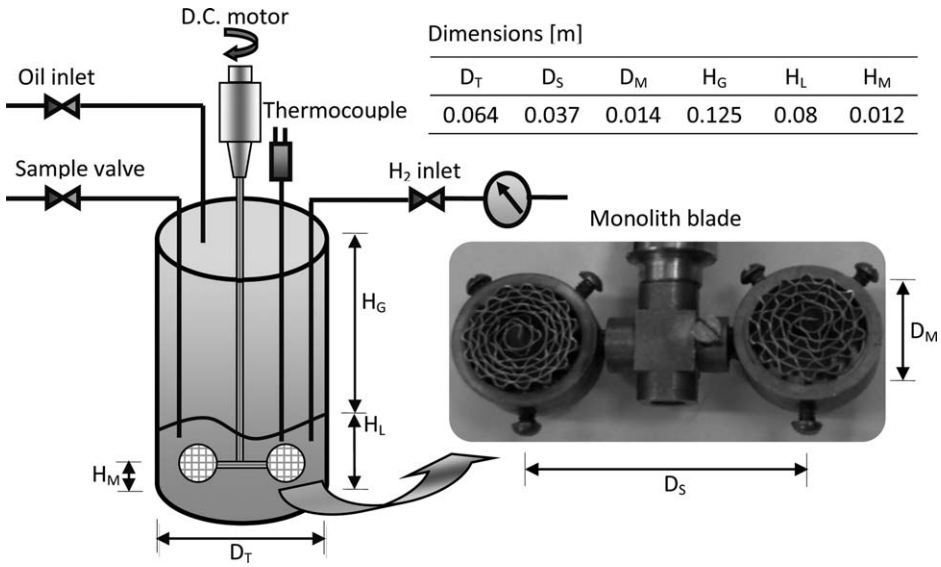

Figure 1. Schematic of the monolithic stirrer reactor.

(plus 40 min pore opening) using a current density of 2 A dm^{-2}.

Monoliths were prepared by rolling around a spindle alternate previously anodized flat and corrugated foils. The final monolith was a cylinder of 14-mm diameter by 15-mm height and a cell density of 55 cells per square centimeter. The monoliths were loaded with Pd by wet impregnation, by dipping them in a $Pd(C_5H_7O_2)_2$ (Fluka, Sigma-Aldrich, 99%) solution in toluene at room temperature for 24 h under agitation. After impregnation, the monoliths were dried at room temperature, and then calcined at 773 K for 2 h. These samples are referred to as $Pd/Al_2O_3/Al$.

Monolithic catalyst characterization

The monolithic catalysts were characterized using N_2 adsorption isotherms at liquid nitrogen temperature for surface area measurements in a Micromeritics ASAP 2000 system. N_2 and He (99.999 % purity) were supplied by Air Liquide.

The amount of alumina generated by the anodizing process was determined by a gravimetrical method. A conventional ultrasonic method was used for the Al_2O_3 adherence test.[18]

The catalyst composition was determined by atomic absorption spectroscopy using a GBC AVANTA Σ unit and x-ray fluorescence in a PANalytical MagiX spectrometer with Rh anode, LiF200, PE, PX1, and PX4 crystals under He atmosphere.

Scanning electron microscopy (JEOL 35 CF, 15 keV voltage of acceleration) and transmission electron microscopy (JEOL 100 CS operated at 100 keV) were used for topographical and particle size studies.

H_2 chemisorption runs were carried out in a conventional pulse apparatus[19] in a special cell at atmospheric pressure and 373 K. Prior to chemisorption, the catalysts were reduced *in situ* at 573 K in flowing H_2 (20 cm^3 min^{-1}). The fraction of exposed Pd was calculated assuming that one hydrogen atom is adsorbed per surface Pd metal atom.

Catalytic activity measurements

The catalytic activity tests were carried out in a 600 cm^3 Parr reactor equipped with a magnetically driven agitator that was modified to perform as a monolithic stirrer (Figure 1). The reaction conditions used are listed in Table 1. Further experimental details on the activity test procedure are given elsewhere.[8]

The reaction products were analyzed by gas chromatography. Triglyceride derivatization for further analysis was carried out following the IUPAC standard method 2.301.[20] Chromatographic analyses were carried out in a HP4890D gas chromatograph using a SUPELCO SP2560 100 m ×

Table 1. Set of Reactions Tested

Test	Temperature (K)	Pressure (kPa)	Catalyst loading ($kg_{Pd,exp}$ m^{-3})	Batch[a]
1	353	414	0.00168	1
2	373	552	0.00168	1
3	353	552	0.00168	1
4	363	483	0.00126	1
5	353	552	0.00084	1
6	373	414	0.00168	1
7	373	414	0.00168	2
8	373	414	0.00168	3
9	373	414	0.00168	4
10	373	414	0.00168	5
11	373	414	0.00168	6
12	373	414	0.00168	7
13	373	414	0.00168	8
14	373	414	0.00168	9
15	373	414	0.00168	10
16	373	414	0.00084	1
17	363	483	0.00126	1
18	373	552	0.00084	1
19	363	483	0.00126	1
20	353	414	0.00084	1
21	373	414	0.00527	1
22	373	414	0.00527	2
23	373	414	0.00527	3
24	373	414	0.00527	4
25	373	414	0.00527	5
26	373	414	0.00527	6
27	373	414	0.00527	7
28	373	414	0.00527	8
29	373	414	0.00527	9
30	373	414	0.00527	10

[a]Number of times that the monolithic catalyst was used in reaction.

Table 2. Kinetic Model, Including Hydrogenation and Geometric Isomerization Reactions

Hydrogenation Reaction	Isomerization Reaction
$C \xrightarrow{k_1} S \quad (r_1)$	$C \overset{k_{iso}}{\leftrightarrow} T \quad (r_{iso})$
$T \xrightarrow{k_1} S \quad (r_1')$	$CC \overset{k_{iso}}{\leftrightarrow} CT \quad (r_{iso}')$
$CC \xrightarrow{k_2} C \quad (r_2)$	$CT \overset{k_{iso}}{\leftrightarrow} TT \quad (r_{iso}'')$
$CT \xrightarrow{k_2} C \quad (r_2')$	
$CT \xrightarrow{k_2} T \quad (r_2'')$	
$TT \xrightarrow{k_2} T \quad (r_2''')$	

0.25 mm × 0.2 mm capillary column. Operating conditions and related procedures followed the AOCS method Ce 1c-89.[21] The fatty acids in the analyzed samples were identified by comparison with the Supelco® 47885-U analytical standard. The iodine index is a measure of unsaturation of triglyceride molecules. Its value decreases as the number of double bonds diminishes, and it can be determined from the chromatographic analysis according to AOCS norm Cd 1c-85.[22]

Two monoliths were arranged as the blades of the agitator, as shown in Figure 1, and reduced *in situ* in a hydrogen flow of 100 cm^3 min^{-1} for 30 min at 373 K. In each reaction, 250 cm^3 of predisoxigenized oil was used. To monitor the reaction progress, 0.5 cm^3 samples were taken every 10 min.

Integral Model of the Monolithic Stirrer Reactor

The monolithic stirrer reactor can be modeled as an ideal semibatch reactor for H_2 and as a batch reactor for the liquid reactant and product. The hypotheses considered for the reactor model were as follows:

- Perfect mixture of reactants and product in the tank (the concentration gradients inside the monolith channels were disregarded).
- Heterogeneous model with resistance in the gas–liquid interface and in the liquid–solid film, considering intraparticle diffusional resistance.
- Isothermal reactor (see Evaluation of diffusional controls section).

Experiences not shown in the present manuscript revealed the high mixing performance of the reactor.

Kinetic model

A model for the hydrogenation reaction of sunflower oil was developed taking into account the hydrogenation of the double bond, and also the isomerization reactions (as shown in Table 2) and the deactivation phenomenon. For the molecular adsorption of the surface hydrogen, a dissociative mechanism was considered.[23]

The kinetic model was based on the following assumptions[24]:

- The triglyceride and H_2 molecules do not compete for the same active sites.
- The amount of vacant sites for triglycerides is negligible.[23,25]
- Triglyceride and H_2 adsorption are assumed to be at equilibrium.
- The fractions of the surface occupied by the intermediates are negligible due to their high reactivity.
- The location of the double bonds does not affect the reaction rates.
- The probability of diene adsorption is twice as much as the monoene adsorption.[24]
- The same overall effectiveness factor is assumed for the different reactions because reaction rates and diffusivities have the same order, thus simplifying the calculation (Overall effectiveness factor section).
- The reaction rate is controlled by adding the first hydrogen in the double bond.[26]

For a well-agitated batch reactor, the mass balances of the species can be written as follows

$$\frac{dC_{CC}}{dt} = \varphi_i \; w \; \eta\left(-r_2 - r_{iso}'\right) \tag{1}$$

$$\frac{dC_{CT}}{dt} = \varphi_i \; w \; \eta\left(-r_2' - r_2'' - r_{iso}'' + r_{iso}'\right) \tag{2}$$

$$\frac{dC_{TT}}{dt} = \varphi_i \; w \; \eta\left(-r_2''' + r_{iso}''\right) \tag{3}$$

$$\frac{dC_C}{dt} = \varphi_i \; w \; \eta\left(r_2 + r_2' - r_1 - r_{iso}\right) \tag{4}$$

$$\frac{dC_T}{dt} = \varphi_i \; w \; \eta\left(r_{iso} - r_1' + r_2'' + r_2'''\right) \tag{5}$$

$$\frac{dC_S}{dt} = \varphi_i \; w \; \eta\left(r_1' + r_1\right) \tag{6}$$

The Langmuir-Hinshelwood (LH) rate expressions can be described by

$$r_2 = k_2 \; \theta_{CC} \; \theta_H \tag{7}$$

$$r_2' = \frac{1}{2} \; k_2 \; \theta_{CT} \; \theta_H \tag{8}$$

$$r_2'' = \frac{1}{2} \; k_2 \; \theta_{CT} \; \theta_H \tag{9}$$

$$r_2''' = k_2 \; \theta_{TT} \; \theta_H \tag{10}$$

$$r_1 = k_1 \; \theta_C \; \theta_H \tag{11}$$

$$r_1' = k_1 \; \theta_T \; \theta_H \tag{12}$$

$$r_{iso} = k_{iso}\left(\theta_C - \frac{\theta_T}{K_{iso}}\right)\theta_H \tag{13}$$

$$r_{iso}' = k_{iso}\left(\theta_{CC} - \frac{\theta_{CT}}{2 \; K_{iso}}\right)\theta_H \tag{14}$$

$$r_{iso}'' = k_{iso} \; \left(\frac{1}{2}\theta_{CT} - \frac{\theta_{TT}}{K_{iso}}\right)\theta_H \tag{15}$$

The $^1/_2$ factor included in Eqs. 8, 9, 14, and 15 considers the possibility that the hydrogenation or isomerization of a certain double bond into a di-unsaturated compound can occur.

The deactivation process is represented by φ_i in Eqs. 1–6, and it is explained in Deactivation section.

The expressions for the vacant sites (θ_i) were obtained considering the kinetic model presented in Table 2 (they are listed as Supporting Information).

Previous reports determined an equilibrium constant value of $K_{iso} = 3.5$ at a temperature of 393 K for the equilibrium between oleic and elaidic acids during reaction.[23]

The kinetic constant k_i and the hydrogen adsorption constant K_H depend on temperature following an Arrhenius-type function.

Deactivation

To reproduce the experimentally observed behavior, the deactivation phenomenon can be expressed as a function that depends on the reaction time (ψ).[27] Besides, there is also a deactivation phenomenon associated with the number of reuses of the catalyst. This deactivation was modeled by a β multiplying parameter, with $\beta = 1$ for the first use of the monolithic catalyst (Batch = 1). Thus, the following three models were analyzed for the catalyst deactivation

$$\varphi_1 = \psi_1 \;\; \beta = \beta \;\; (1 - \alpha t) \tag{16}$$

$$\varphi_2 = \psi_2 \;\; \beta = \beta \;\; \exp(-\alpha t) \tag{17}$$

$$\varphi_3 = \psi_3 \;\; \beta = \frac{\beta}{1 + \alpha \;\; t} \tag{18}$$

The models were denoted by D1 (Eq. 16), D2 (Eq. 17), and D3 (Eq. 18). Thus, the deactivation was separated from the hydrogenation kinetics.

Overall effectiveness factor

In a previous work,[28] a theoretical derivation of the overall effectiveness factor for slab geometry applicable to uniform washcoats on a monolith surface for three-phase reaction systems was developed, based on the work of Ramachandran and Chaudhari.[29,30] The overall effectiveness factor is defined as the ratio of the observed reaction rate (R_H) to the reaction rate without transport resistances (Ω_H) according to the following equation

$$\eta = \frac{R_H}{w \Omega_H (C_{H_2}{}^*)} \tag{19}$$

where

$$R_H = M_H (C_{H_2}{}^* - C_{H_{2S}}) \tag{20}$$

$$\frac{1}{M_H} = \frac{1}{k_{GL} \;\; a_L} + \frac{1}{k_{LS} \;\; a_S} \tag{21}$$

It is worth noting that Ω_G will be expressed according to the type of kinetics adopted. For a LH model

$$\Omega_H = k_0 \theta_H \tag{22}$$

where k_0 is given in Ref. 23.

Equation 19 can be rewritten

$$\eta = \frac{\eta_c \sqrt{1 + K_H \;\; C_{H_2}{}^*} \sqrt{1 - \eta/\sigma_H}}{1 + \sqrt{K_H \;\; C_{H_2}{}^*} \sqrt{1 - \eta/\sigma_H}} \tag{23}$$

where

$$\sigma_H = \frac{M_H \;\; \sqrt{C_{H_2}{}^*} \left(1 + \sqrt{K_H \;\; C_{H_2}{}^*}\right)}{w \;\; k_0 \;\; \sqrt{K_H}} \tag{24}$$

$$\varnothing = \frac{\varnothing_0 \;\; K_H \;\; C_{H_2}{}^* (1 - \eta/\sigma_H)}{\sqrt{2} \;\; [1 + K_H \;\; C_{H_2}{}^* \;\; (1 - \eta/\sigma_H)] \{K_H \;\; C_{H_2}{}^* \;\; (1 - \eta/\sigma_H) - ln[1 + K_H \;\; C_{H_2}{}^* \;\; (1 - \eta/\sigma_H)]\}^{1/2}} \tag{25}$$

$$\eta_c = \frac{\tanh(\varnothing)}{\varnothing} \tag{26}$$

where $\varnothing_0$ can be expressed as

$$\varnothing_0 = L \left(\frac{k_0 \;\; K_H \;\; \rho_c}{D_e} \right)^{1/2} \tag{27}$$

Mathematical tools

The Gproms software was used to solve the set of algebraic and differential equations, and to fit the experimental data. It is based on the statistical method of maximum likelihood estimation.

To perform a direct comparison of the parametric goodness of fit of the different models, the Akaike Information Criterion (AIC) was used.[31] The AIC provides a means for model selection: the model with the minimum AIC value will be the preferred model.

The relative likelihood (RL) is determined by the following function[32]

$$\mathrm{RL} = \exp\left(\frac{\mathrm{AIC}_{\min} - \mathrm{AIC}_i}{2} \right) \tag{28}$$

RL can be understood as the relative probability that the ith model minimizes the estimated information loss.

Evaluation of diffusional controls

The catalytic hydrogenation of vegetable oils is a three-phase system strongly limited by mass-transfer resistances. Boldrini et al.[9] carried out an exhaustive study on the hydrogenation of sunflower oil with a monolithic stirrer reactor, determining the coefficients of internal and external mass transfer under the same conditions as used in the present work.

Mass transfer in the gas–liquid interphase

The coefficient of gas–liquid mass transfer ($k_{GL}a$) was determined by gas absorption measurements according to the technique described by Teramoto et al.[33] For the reaction system used in this work, $k_{GL}a$ presented a value of 0.15 s^{-1}, which was used in the present analysis.[9]

Mass transfer in the liquid–solid film

The coefficient of hydrogen mass transfer in the liquid–solid film was estimated using the Sherwood correlation proposed by Hoek,[34] valid for a three-phase system in a monolithic stirrer reactor, thus obtaining the average mass-transfer coefficient k_{LS}.

$$Sh = \frac{k_{LS} D_H}{D} = 1.16 (Re \;\; Sc)^{1/3} \tag{29}$$

The molecular diffusion of H_2 in oil was obtained from the expression reported by Fillion and Morsi.[35] The density and the viscosity of the liquid were calculated according to Refs. 36 and 37.

The fluid velocity rate inside the channels (required to calculate the Reynolds number) was obtained by the method of Edvinsson et al.[17] For an agitation rate of 1400 rpm, it was found that the average velocity in the monolith channels is a function of temperature determined by

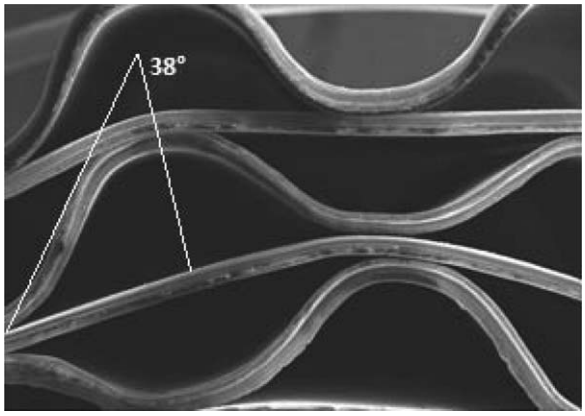

Figure 2. SEM image of the monolith channels: corrugation inclination angle (δ) relative to the vertical axis.

$$V\ \left[\mathrm{m\ s^{-1}}\right]=0.0076\ T[\mathrm{K}]-2.1595 \tag{30}$$

Evaluation of heat transfer

The analysis of heat transfer is very important for highly exothermic hydrogenations.

External diffusion effects of heat

An energy balance between the fluid and the catalyst surface verified that the heat generated by the reaction equals the heat-transfer rate between the catalyst and the fluid.[27] The difference in temperature between the bulk of the fluid and the catalyst surface is given by

$$(T_s-T_B)=\frac{(-\Delta H)R_H W}{h\ a_m} \tag{31}$$

The parameters present in the previous expression can be obtained experimentally, except for the heat-transfer coefficient (h), which can be calculated from the Nusselt number, defined as

$$Nu=\frac{hl}{\lambda_L} \tag{32}$$

A model for predicting the Nu number in the combined entrance region of noncircular channels was developed by Muzychka and Yovanovich based on the Lévêque expression.[38] This model predicts the average Nu number and is valid for isothermal and isoflux boundary conditions. They proposed a general equation valid for any geometry, and different region flows, according to the following expression

$$Nu_{\sqrt{A}}(z^*)=\left[\left\{C_2\ C_3\ \left(\frac{fRe_{\sqrt{A}}}{z^*}\right)^{\frac{1}{3}}\right\}^5+\left\{C_1\ \left(\frac{fRe_{\sqrt{A}}}{8\ \sqrt{\pi}\ \epsilon^{\gamma}}\right)\right\}^5\right]^{1/5} \tag{33}$$

Table 4. RL Values for the Kinetic Models Studied

Kinetic Model	RL
LH-D1	0.99
LH-D2	0.99
LH-D3	1

$$fRe_{\sqrt{A}}=\frac{12}{\sqrt{\epsilon}\ (1+\epsilon)\left[1-\frac{192\epsilon}{\pi^5}\tanh\left(\frac{\pi}{2\epsilon}\right)\right]} \tag{34}$$

$$z^*=\frac{z\ Re_L Pr}{L} \tag{35}$$

The values used for the constants C_1, C_2, and C_3 were 3.24, 1.5, and 0.409, while the parameter γ had a value of 0.1.[38] For the system studied, at 373 K, the thermal (L_T) and hydrodynamic (L_H) entry lengths were 0.26 and 0.003 m, respectively, indicating a Graetz flow ($L >> L_H$, $L << L_T$).

To calculate Pr, the heat capacity of the oil was calculated according to Ref 39, and the thermal conductivity (λ_L) was obtained from Ref. 39.

The characteristic length used in Eq. 32 is $\sqrt{A}$, where A represents the cross-sectional area of the channel. For the sinusoidal channels,[40] the flow area is

$$A=2\,b\,a\cos(\delta) \tag{36}$$

δ is defined as the inclination angle of the corrugated wall to the vertical axis. It was obtained by a direct experimental measurement from the front view of the monolith (Figure 2).

In a previous work, the Lévêque approximation was used for a three-phase system in a monolithic stirrer reactor.[34]

Internal diffusion effects of heat

Based on the simultaneous resolution of the heat and mass balances, disregarding all the external resistances and considering a complete reaction, the following expression is obtained for the maximum intrapore temperature gradient[27]

$$\Delta T_{max}=\frac{(-\Delta H)D_e C_{H_2S}}{\lambda_e} \tag{37}$$

The effective thermal conductivity can be determined using the porosity values and thermal conductivities of the solid and the fluid according to

$$\lambda_e=\lambda_s\left(\frac{\lambda_L}{\lambda_s}\right)^{1-\varepsilon} \tag{38}$$

The thermal conductivity of the solid (λ_s) was approximated to the corresponding value of alpha alumina, given its structural similarities with the alumina generated by anodization, according to the correlation reported in Ref. 41.

The effective diffusivity was calculated based on the properties of the support, considering a tortuosity value of 1 (due to the linear geometry of the pore) and a porosity ($\varepsilon = 0.3$).

The H_2 concentration on the surface corresponds to the level of H_2 solubility in the liquid phase, which was calculated following the equation presented by Fillion and Morsi.[35]

Table 3. Some Morphological Properties of the Anodization Layer of the Monolithic Catalyst

	BET Surface Area				
Mass Al_2O_3 (gm_{Al}^{-2})	(m^2 monolith^{-1})	($m^2 g_{Al2O3}^{-1}$)	Pore Radius (Å)	Al_2O_3 Thickness (μm)	Pore Volume (cm^3 monolith^{-1})
33.82	8	25	220	18	0.012

Table 5. Kinetic Parameters Fitted for the LH-D3 Model with the Corresponding Confidence Intervals of 95%

Parameter	Value
E_1/R (K)	8104.9 ± 20
E_2/R (K)	7911.1 ± 20
E_H/R (K)	1161.9 ± 91
E_{iso}/R (K)	6956.5 ± 20
k_{1_0} (kmol $kg_{Pd,exp}^{-1}s^{-1}$)	0.3415 ± 0.0005
k_{2_0} (kmol $kg_{Pd,exp}^{-1}s^{-1}$)	3.5959 ± 0.0053
k_{iso_0} (kmol $kg_{Pd,exp}^{-1}s^{-1}$)	2.6705 ± 0.0039
K_{H_0} (kmol $kg_{Pd,exp}^{-1}s^{-1}$)	709.474 ± 5
α (dimensionless)	$1.9 \times 10^{-6} \pm 7.7 \times 10^{-8}$

Thus, the variation of maximum temperature inside the pores of the catalyst could be determined.

Results and Discussion

The morphological characteristics of the alumina support acquired by the anodization process are presented in Table 3. No weight loss was observed in the adherence test of the monoliths analyzed, indicating that the alumina generated by anodization has a high adherence to the substrate. The TEM images showed that the Pd particles had a diameter of 5 nm, representing a metallic dispersion of 35%.

Regarding heat transfer, it was evaluated at $T = 373$ K with a catalyst loading = 0.00527 $kg_{Pd,exp}$ m^{-3} (conditions of the highest activity) considering the following values $-\Delta H = -121$ kJ mol^{-1}, R_H=699mol $s^{-1}kg_{cat}^{-1}$.

The effects of internal heat transfer were evaluated using Eq. 37, with $\lambda_e = 0.5$ W m^{-2} K^{-1}. The difference in intraparticle temperature was approximately 0.003 K. Heat external diffusion effects were analyzed taking into account Eq. 31, with $h = 1025$ W m^{-2} K^{-1}, $a_m = 0.0168$ m^2. The calculations show a negligible temperature increase of 1.6 K between the bulk liquid and the catalyst surface; therefore, the system operated under isothermal conditions.

The RL values for all the proposed models are presented in Table 4. It was found that the model LH-D3 (LH mechanism and deactivation kinetics described by Model 3) presented the minimum AIC value, representing the experimental data with the highest precision. The numerical difference in RL was of 0.01, which would indicate that there was no significant difference between the deactivation models. This point will be further discussed later.

The kinetic parameters fitted for the kinetic model LH-D3 are shown in Table 5.

It can be observed that the kinetic constant k_{i_0} of the hydrogenation of diene (3.5959kmol $kg_{Pd,exp}^{-1}s^{-1}$) was higher than that of monoene (0.3415kmol $kg_{Pd,exp}^{-1}s^{-1}$), whereas their corresponding activation energies showed the opposite behavior (7911 and 8105 J mol^{-1}, respectively), confirming that the hydrogenation of diene has a higher activation rate than monoene.

Regarding the activation energy of the isomerization reaction, the value was noticeably lower than those corresponding to the hydrogenation reactions, which indicates that the effect of temperature is differential.

In the case of the value obtained for the constant of H_2 adsorption on the catalyst surface, once again the results were in agreement with the literature.[23] The activation energy associated with this parameter was low, showing a low temperature dependence.

The values obtained for the kinetic parameters can be compared with those reported in the literature. Santacesaria et al.[23] and Fernández et al.[24] studied the hydrogenation of

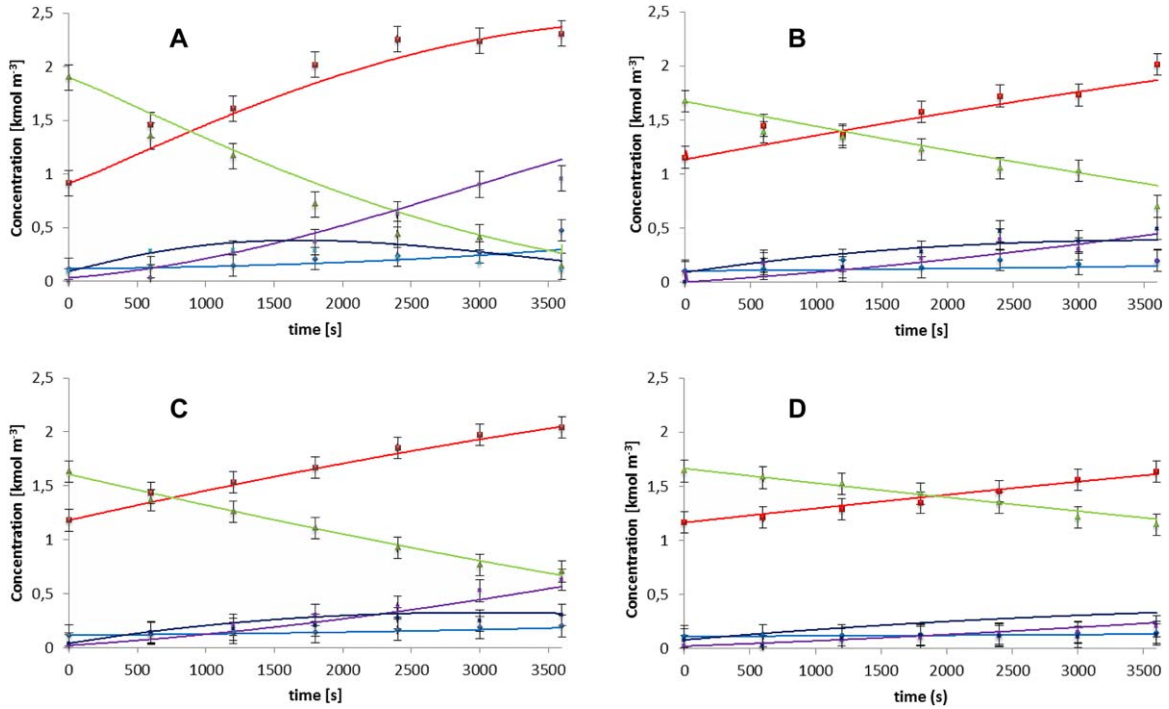

Figure 3. Hydrogenation of sunflower oil.

Operating conditions: (A) $T = 373$ K, metallic loading = 0.00168 $kg_{Pd,exp}$ m^{-3}; (B) $T = 353$ K, metallic loading = 0.00168 $kg_{Pd,exp}$ m^{-3}; (C) $T = 373$ K, metallic loading = 0.00084 $kg_{Pd,exp}$ m^{-3}; (D) $T = 353$ K, metallic loading = 0.00084 $kg_{Pd,exp}$ m^{-3}. References: Curves: simulation, Dots: experimental data, ◆ C18:0; ■ C18:1; X Trans C18:1; ▲ C18:2; * Trans C18:2. [Color figure can be viewed in the online issue, which is available at wileyonlinelibrary.com.]

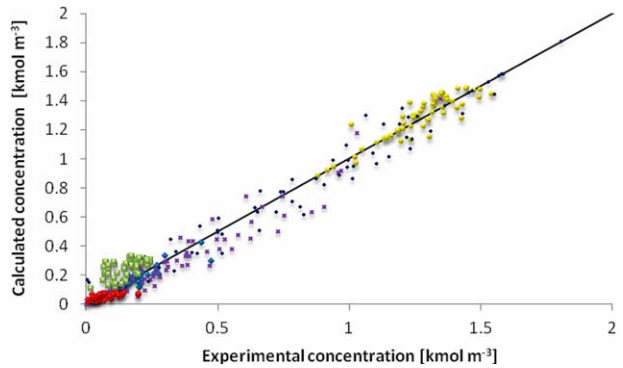

Figure 4. Parity plot of the calculated vs. experimental concentrations for the LH-D3 model.

References: ◆ C18:0, ■ C18:2 CCT, ▲ C18:2 CTT, + C18:2 CCC, XC18:1 CT, ○ C18:1 CC. [Color figure can be viewed in the online issue, which is available at wileyonlinelibrary.com.]

sunflower oil on palladium catalysts supported over slurry-type systems, reporting similar values for the kinetic constants to those found in the present work (8 and 1 kmol $kg^{-1}_{pd,exp}s^{-1}$ and 0.39 and 0.1 for k_{2_0} and k_{1_0}, respectively).

A good fit of the kinetic parameters would show the goodness of the mathematical model of the reactor, and the adequate determination of the mass-transfer coefficients.

The experimental and calculated concentration profiles for the model LH-D3 are shown in Figure 3. Figure 3A presents the tests carried out at 373 K and 414 kPa with a metallic loading of 0.00168 $kg_{Pd,exp}$ m^{-3}, and Figure 3C corresponds to the same temperature and pressure with a metallic loading of 0.00084 $kg_{Pd,exp}$ m^{-3}. Figures 3B, D correspond to the tests performed at 353 K and 414 kPa with metallic loadings of 0.00168 and 0.00084 $kg_{Pd,exp}$ m^{-3}, respectively. It can be observed that the model describes satisfactorily the hydrogenation kinetics for the configuration of a monolithic stirrer reactor. This is confirmed in Figure 4 for all the experimental tests.

Regarding the deactivation process, as indicated above, no differences were found in the RL values between the proposed models. The models (Eqs. 16–18) considered two independent deactivation phenomena: one associated with the reaction time ($\psi_i = f(\alpha, t)$), and the other one with the

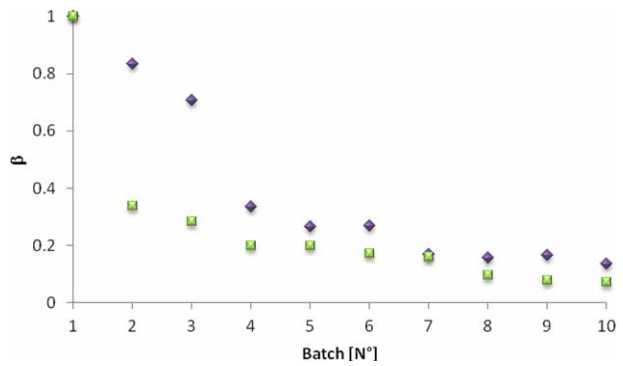

Figure 5. Evolution of parameter β as a function of the number of uses.

Operating conditions: (◆) $T = 373$ K, $P = 414$ kPa, metallic loading = 0.00527 $kg_{Pd,exp}$ m^{-3}, (■) $T = 373$ K, $P = 414$ kPa, metallic loading = 0.00168 $kg_{Pd,exp}$ m^{-3}. [Color figure can be viewed in the online issue, which is available at wileyonlinelibrary.com.]

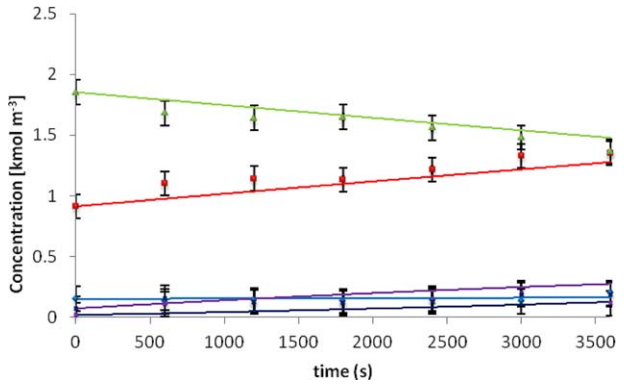

Figure 6. Hydrogenation reaction of sunflower oil corresponding to Batch 3, at $T = 373$ K, $P = 414$ kPa, metallic loading = 0.00168 $kg_{Pd,exp}$ m^{-3}.

Curves = simulation, Dots = experimental data: ◆ C18:0; ■ C18:1; X Trans C18:1; ▲C18:2; * Trans C18:2. [Color figure can be viewed in the online issue, which is available at wileyonlinelibrary.com.]

batch number (β). For the model LH-D3, α presented a value of 1.9×10^{-6}. For the rest of the models, parameter α showed similar values. Figure 5 presents the value of parameter β for the different batches (Pd loading: 0.00168 and 0.00527 $kg_{Pd,exp}$ m^{-3}). For the high Pd loading, this parameter presented values between 0.83 and 0.13 for Batch 2 and 10. For the low Pd loading, β presented lower values, which could be attributed to the extremely low Pd:oil ratio, close to phospholipids concentration in a refined oil.[42] The goodness of fit of the model for the experimental data of Batch 3 is presented in Figure 6 (Test 8 in Table 1).

The physical meaning of Eqs. 16–18 could be associated with the loss of dispersion of the palladium particles (determined by H_2 chemisorption). The decrease in Pd dispersion was not a consequence of sintering of the active metal particles. The TEM micrograph indicated that the mean diameter of the metallic particles remained constant. Thus, the loss of dispersion was due to the coverage of the Pd surface (the specific surface area of the support remained constant). For the test performed at 373 K with 0.00168 $kg_{Pd,exp}$ m^{-3}, β decreased by 90% and Pd dispersion by 84% (between Batches 1 and 10).

In summary, the results of the deactivation model would indicate that the fall in the catalyst activity occurs during reaction and between batches, due to fouling and to catalyst manipulation between batches. The exact contribution of each terms is not fully establish yet. Experimentally, it could be explained by the possible formation of polymers on the Pd surface, which are very difficult to extract with solvent.[8] Polyunsaturated fatty acids are very susceptible to thermal polymerization[43] and oligomer formation caused by oxidation.[44] Metals can act as a catalyst for both polymerizations.[45,46]

To show the usefulness of the mathematical model of the reactor, simulations for four consecutive batches are presented, with the objective of obtaining a final product with IV = 75 (39% C═C conversion) operating with a catalyst loading of 0.00527 $kg_{Pd,exp}$ m^{-3}. The results for the two selected use strategies are presented in Table 6. In the first case (Simulation 1), the first batch was operated at 358 K, and temperature was increased 5 K in subsequent batches. It can be observed that in the first three runs, the reaction times are similar (~1 h): the temperature increase is sufficient to

Table 6. Simulation Results Obtained with the Mathematical Model of the Monolithic Stirrer Reactor for IV = 75 and 0.00527 $kg_{Pd,exp}$ m^{-3}

	Simulation 1				Simulation 2			
			C18:0	*Trans*[a]			C18:0	*Trans*[a]
Batch	T (K)	t_{RX} (h)	(kmol m^{-3})		T (K)	t_{RX} (h)	(kmol m^{-3})	
1	358	0.9	0.33	1.44	373	0.7	0.34	1.36
2	363	1.0	0.34	1.42	373	0.8	0.33	1.36
3	368	1.0	0.33	1.39	373	0.9	0.34	1.36
4	373	2.0	0.34	1.37	373	2.0	0.33	1.36

[a]Total *trans* concentration.

compensate for the loss in catalyst activity. By the fourth use, when the deactivation process is more pronounced, the reaction time is 2 h. Variations in the concentrations of saturated product and total trans isomers are small and result from the different combinations of temperature, time, and catalyst loading variables (as indicated above, the fall in Pd dispersion was confirmed experimentally).[24]

In the second case (Simulation 2), the four batches were operated at 373 K and the reaction time was modified to obtain a hydrogenated oil with IV = 75. In the first three batches, time was increased gradually to reach that objective, whereas in the last run the results were the same as for Simulation 1.

When the results are compared, the sum of the operating times is 5 and 4.4 h for Simulations 1 and 2, respectively. A simple energetic analysis (considering reaction times and temperatures) shows that the operating strategies used in Simulation 2 result in a 5% decrease in energy consumption compared with Simulation 1.

The mathematical model is a very useful and versatile tool to generate usage strategies for the reactor to obtain a given product (by describing the composition) and predict the operating costs of the system (associated with temperature and reaction time for a given catalyst loading).

In this context, Figure 5 could be visualized as function of processed oil volume per mass of catalyst. This concept is probably more relevant for technologies comparison.

Conclusions

A complete mathematical model of a reactor was developed, including hydrogenation and isomerization kinetics, catalyst deactivation, external gas–liquid, and liquid–solid as well as internal mass transfer. The experimental studies were carried out in a $Pd/Al_2O_3/Al$ monolithic stirrer reactor at a wide range of temperatures, pressures, and catalyst loadings.

The good fit of the kinetic parameters indicated the goodness of the mathematical model of the reactor, and the adequate determination of the mass-transfer coefficients.

The mathematical model showed to be a very useful and versatile tool to generate usage strategies for the reactor to obtain a given product (by describing the composition) and to predict the operating costs of the system (associated with reaction temperature and time for a given catalyst loading).

Acknowledgment

The authors thank the Agencia Nacional de Promoción Científica y Tecnológica (National Agency of Scientific and Technological Promotion, Argentina) and the Consejo Nacional de Investigaciones Científicas y Técnicas (National Council for Scientific and Technological Research, CONICET) for their financial support.

Notation

a = major length of channel, m
A = flow area, m^2
a_L = gas − liquid interfacial area per unit volume of liquid, m^2_{GL} m_L^{-3}
a_m = geometrical surface area of monolith, m^2
a_S = liquid − solid interfacial area, m^2
b = minor length of channel, m
C_j = concentration of component j, kmol m^{-3}
$C^*_{H_2}$ = hydrogen bulk − oil concentration, kmol m^{-3}
$C_{H_{2S}}$ = concentration of H_2 at the catalyst surface, mol m^{-3}
Cp = Heat capacity, J kg^{-1} K^{-1}
D = diffusivity, m^2 s^{-1}
D_e = effective diffusivity, m^2 s^{-1}
D_H = hydraulic diameter, m
E_i = energy of activation, kJ $kmol^{-1}$
h = heat- transfer coefficient, W m^{-2} K^{-1}
ΔH = heat of reaction, J $mol^{-1}_{H_2}$
K_j = adsorption constant for j compound, m^3 $kmol^{-1}$
K_{iso} = isomerization equilibrium constant, m^3 $kmol^{-1}$
k_{GL} = gas − liquid mass-transfer coefficient, m^3_L $m^{-2}_{GL}s$
k_i = kinetic constant, $kmol^{-1}$ kg^{-1} s^{-1}
k_{i_0} = frequency factor, $kmol^{-1}$ kg^{-1} s^{-1}
k_0 = rate constant, $kmol^{-1}$ kg^{-1} s^{-1}
k_{LS} = liquid − solid mass-transfer coefficient, m s^{-1}
$l = \sqrt{A}$ = characteristic length, m
L = thickness of the catalytic slab, m
L_C = length of channel, m
M_H = total mass-transfer resistances, s^{-1}
Nu = Nusselt number, dimensionless
$Pr = Cp\ \frac{\mu}{\lambda_L}$ = Prandtl number, dimensionless
r_i = reaction rate, $kmol^{-1}$ kg^{-1} s^{-1}
R = 8.314 = gas constant, J $kmol^{-1}$ kg^{-1}
$Re = \frac{\rho_L V D_H}{\mu}$ = Reynolds number, dimensionless
R_H = observed rate of reaction of hydrogen, $kmol^{-1}$ s^{-1} m^{-3}
$Sc = \frac{\mu}{\rho}\ D$ = Schmidt number, dimensionless
Sh = Sherwood number, dimensionless
t = time, s
T = temperature, K
T_s = temperature at catalyst surface, K
T_B = bulk fluid temperature, K
ΔT_{max} = maximum intrapore temperature gradient, K
V = linear velocity in monolith channel m s^{-1}
w = mass of catalyst per unit volume of liquid, kg m^{-3}
W = mass of catalyst, kg

Greek letters

β = multiplying parameter related to batch deactivation
γ = shape parameter, dimensionless
δ = corrugation inclination angle, °
ε = porosity, m^3_{liq} m^{-3}_{cat}

$\epsilon = \frac{b}{a}$ = appearance ratio,dimensionless
η = overall effectiveness factor,dimensionless
η_c = catalytic effectiveness factor,dimensionless
θ_j = surface coverage fraction of component *j*,dimensionless
λ_e = effective thermal conductivity of solid,J m^{-1} s^{-1} K^{-1}
λ_L = thermal conductivity of liquid,J m^{-1} s^{-1} K^{-1}
λ_s = thermal conductivity of solid,J m^{-1} s^{-1} K^{-1}
μ = viscosity,kg m^{-1} s^{-1}
ρ_c = density of the catalyst, kg m^{-3}
ρ_L = density of liquid, kg m^{-3}
σ_G = parameter defined by Eq. 32, dimensionless
φ_i = function describing deactivation phenomenon
ϕ = generalized Thiele modulus, dimensionless
ϕ_0 = Thiele modulus, dimensionless
ψ = activity function
Ω_H = local rate of chemical reaction per unit weight of catalyst, $kmol^{-1}$ kg^{-1} s^{-1}

Subscripts

C = *cis* geometric isomer of monoene
CC = diene having two double bonds in *cis* position
j = *C*, *CC*, *CT*, *H*, *S*, *T*, and *TT*
S = saturated
T = *trans* geometric isomer of monoene
TT = diene having two double bonds in *trans* position

Literature Cited

1. Cybulski A, Moulijn JA. Monoliths in heterogeneous catalysis. *Catal Rev Sci Eng*. 1994;36(2):179–270.
2. Kapteijn F, Nijhuis TA, Heiszwolf JJ, Moulijn JA. New non-traditional multiphase catalytic reactor based on monolithic structures. *Catal Today*. 2001;66(2–4):133–144.
3. Bussard AG, Waghmare YG, Dooley KM, Knopf FC. Hydrogenation of α-methylstyrene in a piston-oscillating monolith reactor. *Ind Eng Chem Res*. 2008;47(14):4623–4631.
4. Nijhuis T, Kreutzer M, Romijn A, Kapteijn F, Moulijn JA. Monolithic catalysts as efficient three-phase reactors. *Chem Eng Sci*. 2001; 56(3):823–829.
5. Marwan H, Winterbottom JM. The selective hydrogenation of butyne-1,4-diol by supported palladiums: a comparative study on slurry, fixed bed, and monolith downflow bubble column reactors. *Catal Today*. 2004;97(4):325–330.
6. Boger T, Zieverink M, Kreutzer M, Kapteijn F, Moulijn J, Addiego W. Monolithic catalysts as an alternative to slurry systems: hydrogenation of edible oil. *Ind Eng Chem Res*. 2004;43: 2337–2344.
7. Sánchez MJF, González Bello OJ, Montes M, Tonetto GM, Damiani DE. Pd/Al_2O_3-cordierite and Pd/Al_2O_3-Fecralloy monolithic catalysts for the hydrogenation of sunflower oil. *Catal Commun*. 2009;10: 1446–1449.
8. Sánchez MJF, Boldrini D, Tonetto GM, Damiani DE. Palladium catalyst on anodized aluminum monoliths for the partial hydrogenation of vegetable oil. *Chem Eng J*. 2011;167:355–361.
9. Boldrini DE, Sánchez MJF, Tonetto GM, Damiani DE. Monolithic stirrer reactor: performance in the partial hydrogenation of sunflower oil. *Ind Eng Chem Res*. 2012;51(38):12222–12232.
10. Lee KW, Mei B, Bo Q, Kim YW, Chung KW, Han Y. Catalytic selective hydrogenation of soybean oil for industrial intermediates. *J Ind Eng Chem*. 2007;13(4):530–536.
11. Nohair B, Especel C, Lafaye G, Marecot P, Hoang LC, Barbier J. Palladium supported catalysts for the selective hydrogenation of sunflower oil. *J Mol Catal A: Chem*. 2005; 229(1–2):117–126.
12. Edgar BC. Modifying vegetable oils for food and non-food purposes. In: Vollmann J, Rajcan I, editors. *Oil Crops, Handbook of Plant Breeding*, Vol. 4. Springer, New York, USA, 2009:31–56.
13. Ramachandran PA, Chaudhari RV. *Three Phase Catalytic Reactors*. Gordon and Breach, London, UK, 1983.
14. Boger T, Roy S, Heibel AK, Borchers OA. Monolith loop reactor as an alternative to slurry reactors. *Catal Today*. 2003;79–80: 441–451.
15. Broekhuis RR, Machado RM, Nordquist AF. The ejector-driven monolith loop reactor: experiments and modeling. *Catal Today*. 2001;69(1–4):87–93.
16. Heiszwolf JJ, Engelvaart LB, van den Eijnden MG, Kreutzer MT, Kapteijn F, Moulijn JA. Hydrodynamic aspects of the monolith loop reactor. *Chem Eng Sci*. 2001;56:805–812.
17. Edvinsson-Albers RK, Houterman MJJ, Vergunst T, Grolman E, Moulijn JA. Novel monolithic stirrer reactor. *AlChE J*. 1998;44(11): 2459–2464.
18. Zhao S, Zhang J, Weng D, Xu X. A method to form well-adhered δ-Al_2O_3 layers on FeCrAl metallic supports. *Surf Coat Technol*. 2003;167:97–105.
19. Konopny L, Juan A, Damiani D. Preparation and characterization of γ-Al_2O_3-supported PdMo catalysts. *Appl Catal B*. 1998;15:115–127.
20. IUPAC. Standard Method 2.301: preparation of fatty acid metil ester. *Standard Methods for the Analysis of Oils, Fat and Derivatives*. Oxford: Blackwell, 1987.
21. AOCS. Official Method Ce 1c-89. Sampling and analysis of commercial fats and oils. Fatty acid composition by GLC cis,cis and trans isomers. AOCS, Champaign, USA, 1993.
22. AOCS. Official Method Ce 1c-85. Sampling and analysis of commercial fats and oils. Calculated iodine value. AOCS, Champaign, USA, 2009.
23. Santacesaria E, Parella P, Di Serio M, Borelli G. Role of mass transfer and kinetics in the hydrogenation of rapeseed oil on a supported palladium catalyst. *Appl Catal A*. 1994; 116:269–294.
24. Fernández M, Tonetto G, Capriste G, Damiani D. Kinetics of the hydrogenation of sunflower oil over alumina supported palladium catalyst. *Int J Chem React Eng*. 2007;5:1–22.
25. Rodrigo MT, Daza L, Mendioroz S. Nickel supported on natural silicates. Activity and selectivity in sunflower seed oil hydrogenation. *Appl Catal A*.1992;88:101–114.
26. Jonker GH, Veldsink JW, Beenackers AA. Intrinsic kinetics of 9-monoenic fatty acid methyl esters hydrogenation over nickel-based catalyst. *Ind Eng Chem Res*.1997;36:1567–1579.
27. Froment GF, Bischoff KB. *Chemical Reactor Analysis and Design*, 2nd ed. New York: Wiley, 1990.
28. Boldrini DE, Tonetto GM, Damiani DE. Overall effectiveness factor for slab geometry in a three-phase reaction system. *Int J Chem React Eng*. 2014;12(1):1–11.
29. Chaudhari RV, Ramachandran PA. Influence of mass transfer on zero-order reaction in a catalytic slurry reactor. *Ind Eng Chem Fundam*. 1980;19:201–206.
30. Chaudhari RV, Ramachandran PA. Three phase slurry reactors. *AIChE J*. 1980;26(2):177–201.
31. Akaike H. A new look at the statistical model identification. *IEEE Trans Autom Control*. 1976;19(6):716–723.
32. Burnham KP, Anderson DR. *Model Selection and Multimodel Inference: A Practical Information-Theoretic Approach*, 2nd ed. Springer-Verlag, New York, USA, 2002.
33. Teramoto M, Tai S, Nishii K, Teranishi H. Effects of pressure on liquid-phase mass transfer coefficients. *Chem Eng J*. 1974;8(3):223–226.
34. Hoek I. Towards the catalytic application of a monolithic stirrer reactor. Ph.D. Thesis. Delft, The Netherlands: Technische Universiteit Delft, 2004.
35. Fillion B, Morsi BI. Kinetics, gas−liquid mass transfer, and modeling of the soybean oil hydrogenation process. *Ind Eng Chem Res*. 2002;41(4):697–709.
36. Esteban B, Riba J, Baquero G, Rius A, Puig R. Temperature dependence of density and viscosity of vegetable oils. *Biomass Bioenergy*. 2012;42:164–171.
37. Noureddini H, Teoh B, Clements L. Viscosities of vegetable oils and fatty acids. *J Am Oil Chem Soc*. 1992;69:1189–1191.
38. Muzychka YS, Yovanovich MM. Laminar forced convection heat transfer in the combined entry region of non-circular ducts. *J Heat Transfer*. 2004;126(1):54–61.
39. Garcia Rojas EE, Coimbra JSR, Telis Romero J. Thermophysical properties of cotton, canola, sunflower and soybean oils as a function of temperature. *Int J Food Prop*. 2013;16(7):1620–1629.
40. Dovic D, Palm B, Svaic S. Generalized correlations for predicting heat transfer and pressure drop in plate heat exchanger channels of arbitrary geometry. *Int J Heat Mass Transfer*. 2009;52(19–20):4553–4563.
41. Auerkari P. Mechanical and physical properties of engineering alumina ceramics. Research Notes. PB97–153134. Technical Research Center of Finland, Otaniemi, Finland, 1996.
42. Zufarov O, Schmidt S, Sekretár S. Degumming of rapeseed and sunflower oils. *Acta Chim Slovaca*. 2008;1:321–328.

43. Wang C, Erhan S. Studies of thermal polymerization of vegetable oils with a differential scanning calorimeter. *J Am Oil Chem Soc*. 1999;76(10):1211–1216.
44. Topallar H, Bayrak Y, IscanM. Kinetics of autoxidative polymerization of sunflowerseed oil. *Turk J Chem*. 1997;21(2): 118–125.
45. Fox NJ, Stachowiak GW. Vegetable oil-based lubricants - a review of oxidation. *Tribol Int*. 2007;40:1035–1046.
46. Paz I, Molero M. Catalytic effect of solid metals on thermal stability of olive oils. *J Am Oil Chem Soc*. 2000;77(2):127–130.

Manuscript received Apr. 10, 2014, and revision received June 6, 2014.